Wind and Structures, *Vol. 19, No. 1 (2014) 59-73*
DOI: http://dx.doi.org/10.12989/was.2014.19.1.059

Wind load on irregular plan shaped tall building – a case study

Souvik Chakraborty[1a], Sujit Kumar Dalui[*2] and Ashok Kumar Ahuja[3b]

[1]*Bengal Engineering and Science University Shibpur, India*
[2]*Faculty of Engineering (Civil), Bengal Engineering and Science University, Shibpur, India*
[3]*Faculty of Engineering (Civil), Indian Institute of Technology Roorkee, India*

(Received October 18, 2012, Revised April 14, 2014, Accepted April 19, 2014)

Abstract. This paper presents the results of wind tunnel studies and numerical studies on a '+' plan shaped tall building. The experiment was carried out in an open circuit wind tunnel on a 1:300 scale rigid model. The mean wind pressure coefficients on all the surfaces were studied for wind incidence angle of 0˚ and 45˚. Certain faces were subjected to peculiar pressure distribution due to irregular formation of eddies caused by the separation of wind flow. Moreover, commercial CFD packages of ANSYS were used to demonstrate the flow pattern around the model and pressure distribution on various faces. k-ε and SST viscosity models were used for numerical study to simulate the wind flow. Although there are some differences on certain wall faces, the numerical result is having a good agreement with the experimental results for both wind incidence angle.

Keywords: tall building; computational fluid dynamics (CFD); vortex shedding; pressure coefficients; wind tunnel testing; wind incidence angle

1. Introduction

The uncertainty regarding calculation of wind load is quite high due to the vast ranges of possible interactions between structure and wind. Although the information available in relevant standards on wind loads in different countries (NZS: 1170.2 (2002), ASCE: 7-02 (2002), IS: 875 (Part 3): 1987, NBC (Part 4) (1995)) are sufficient to calculate wind load for regular plan shaped buildings, no such direct databases for irregular plan shaped buildings are available. The developments of new building materials and construction techniques have enabled us to build new buildings which are tall and unsymmetrical. Naturally such structures are more susceptible to wind loads. Thus, it becomes absolutely necessary to estimate wind loads with higher degree of confidence. A structure, under the action of wind, experiences two types of forces viz. drag and lift. While drag force is experienced along the direction of flow, later occurs perpendicular to it.

The velocity (V) at any point of time (t) can be expressed as summation of a static component ($\bar{V}$) and a dynamic component (V_{rms}) (Eq. (1)) (Simiu and Scanlan 1996, Stathopoulos and Baniotopoulos 2007).

∗Corresponding author, Assistant Professor, E-mail: sujit_dalui@rediffmail.com
[a] Post Graduate Student, Email: csouvik41@gmail.com
[b] Professor, Email: ahuja_ak@rediffmail.com

http://www.techno-press.org/?journal=was&subpage=8 ISSN: 1226-6116 (Print), 1598-6225 (Online)

$$V(t) = \overline{V} + V_{rms}(t) \tag{1}$$

For slender and tall structures dynamic responses arises due to phenomenon such as vortex shedding, buffering, galloping and flutter resulting in the increase of complexity of wind loading.

There have been fairly good amount of studies on tall buildings. Kwok (1988) studied the effect of building shape on wind induced response and suggested that horizontal slots, slotted corners and chamfered corners caused significant reductions in both the along-wind and cross-wind responses. Davenport (1993) studied the response of slender structure when subjected to wind loads. Zhou *et al*. (2002) investigated the along wind load on tall building using different international codes. It was suggested that the scatter occurring in calculation of wind load is mainly due to the variation in definition of wind load characteristics. Lin *et al*. (2004) discussed the finding of a wide spread wind-tunnel study on local wind forces on isolated tall buildings based on experimental outcome of nine square and rectangular models (1:500). The effects of elevation, aspect ratio and side ratio on the bluff body flow and on local wind forces were discussed. Gomes *et al*. (2005) enumerated the effect of wind force on L and U shaped models for wind angles varying within 0˚-180˚. The results demonstrated huge difference in response of L and U shaped models as compared to a regular cubical model. Blocken and Carmeliet (2005) carried out wind driven rain measurement on low rise building. The results obtained using computational fluid dynamics package was compared with wind tunnel results. Balendra *et al*. (2005) developed a new technique (Laser Positioning Technique) for computing displacements of buildings. Kim *et al*. (2008) conferred the effects of the tapper ratio and the damping ratio on reducing the across-wind excitation of tall buildings by increasingly reduced velocity. The paper concluded that it was better to increase damping ratio than to increase tapering ratio to reduce the RMS across wind response. Fu *et al*. (2008) enumerated field measurements of the characteristics of boundary layer and storm response of two super tall buildings. The wind tunnel data showed good convergence with the field data.

Gu (2009) carried out wind tunnel test on 27 models of typical tall buildings by wind pressure scanning and HFFB techniques. A new concept of “mode coupling factor” and a modified SRSS method for wind response and equivalent static wind load of complicated tall buildings and structures with consideration of multi-mode contributions and their coupling effects were presented in this paper. Dagnew *et al*. (2009) investigated wind pressure on rectangular plan shaped tall buildings using RANS and LES method. The interference effect of buildings was also simulated. Braun and Awruch (2009) carried out simulation of the wind action over the CAARC (Commonwealth Advisory Aeronautical Council) standard tall building model. The results obtained by numerical and experimental methods displayed good convergence. Revuz *et al.* (2012), after carrying out numerical simulation on a model by varying the domain size, suggested that even for comparatively small domain size, the loss in accuracy is only 10%. Amin and Ahuja (2012) investigated the interference effects between two closely spaced buildings in geometric configuration of ‘L’ and ‘T’ shape for various wind angles. Other works carried out in the field of wind engineering include but are not limited to wind-induced natural ventilation (Cheng *et al*. (2011)), wind resource assessment (Song *et al*. (2014)), wind effect on bridges (Kwok *et al*. (2012)) and reliability based design optimization of structured subjected to wind load (Spence and Gioffre (2012)).

However, due to complexity in wind flow for irregular plan shaped tall structures, most of the investigations carried out till date are focussed on regular plan shaped tall structures. This paper mainly focuses on wind pressures as reflected by wind pressure coefficients on '+' plan shaped tall building for wind incident angle of 0˚ and 45˚. Commercial CFD packages of ANSYS are used for modelling the domain and studying the wind flow. The results obtained from ANSYS are compared with results obtained from actual wind tunnel testing.

2. Experimental program

The experiment was conducted in the Boundary layer wind tunnel having dimension 2.0 m ×2.0 m× 38.0 m at Wind Engineering Centre, Department of Civil Engineering (IIT Roorkee), India. The experimental flow was simulated similar to that of terrain category 2, which corresponds to open terrain with well scattered obstructions having heights generally between 1.5 to 10 m, as per Indian standard for wind load IS: 875 (part 3) - 1987 at a geometric scale of 1:300. The upstream velocity of wind in the wind tunnel, at 1m height, was 10 m/s and turbulence intensity was 10%. Models were placed at a distance of 12 m from upstream side. A reference pitot tube is located at a distance of 10.5 m from grid to measure free stream velocity during experiment.

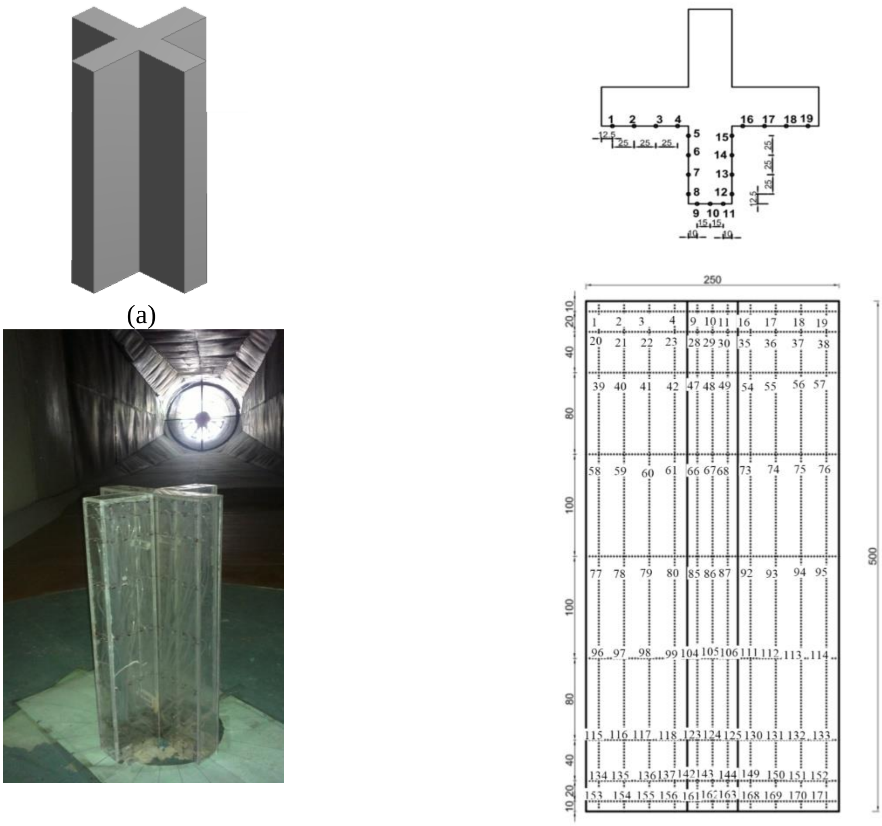

Fig. 1(a) Isometric view of model, (b) Model inside wind tunnel and (c) Plan and elevation of building along with pressure tapping points

The model was made of perspex sheet having a thickness of 4 mm. A total 396 pressure tapping points were placed at nine different levels of 10, 30, 70, 150, 250, 350, 430, 470, 490 mm (Figs. 1(b) and 1(c)). The pressure tapping points were kept near the wall boundaries in order to capture the high pressure variation occurring at point of flow separation. The blockage caused by the model was less than 5% and hence no blockage correction was required. The isometric view, experimental model and plan and elevation of the model along with the location of pressure tapping points are shown in Figs. 1(a)-1(c) respectively.

Readings were taken for wind angle of 0° and 45°. Fig. 2 shows the different faces of the model along with the two wind incident angle (θ).

3. Numerical study

Numerical studies were carried out using two Computational Fluid Dynamics (CFD) packages of ANSYS. A domain having 5H upwind fetch, 15H downwind fetch, 5H top clearance and 5H side clearance, where H is the height of the model has been considered (Franke *et al*. 2004) as shown in Fig. 3(a). A combination of tetrahedral and hexahedral elements was considered for meshing the domain as well as the surface of the building as shown in Fig. 3(b). Two numerical models, namely k-ε and SST were used to simulate the turbulence. The governing equations behind the realizable k-ε model are given by Eqs. (2) and (3)

$$\frac{\partial}{\partial t}(\rho k)+\frac{\partial}{\partial x_j}(\rho k u_j)=\frac{\partial}{\partial x_j}[(\mu+\frac{\mu_t}{\sigma_k})\frac{\partial k}{\partial x_j}]+G_k+G_b-\rho\varepsilon-Y_M+S_k \tag{2}$$

$$\frac{\partial}{\partial t}(\rho\varepsilon)+\frac{\partial}{\partial x_j}(\rho\varepsilon u_j)=\frac{\partial}{\partial x_j}[(\mu+\frac{\mu_t}{\sigma_\varepsilon})\frac{\partial\varepsilon}{\partial x_j}]+\rho C_1 S\varepsilon-\rho C_2\frac{\varepsilon^2}{k+\sqrt{\nu\varepsilon}}+C_{1\varepsilon}\frac{\varepsilon}{k}C_{3\varepsilon}G_b+S_\varepsilon \tag{3}$$

Where,

$$C_1=\max[0.43,\frac{n}{n+5}],n=S\frac{k}{\varepsilon},S=\sqrt{2S_{ij}S_{ij}}$$

G_k represents the generation of turbulence kinetic energy due to the mean velocity gradients, G_b is the generation of turbulence kinetic energy due to buoyancy and Y_m represents the contribution of the fluctuating dilatation in compressible turbulence to the overall dissipation rate, C_1 and C_2 are constants. σ_k and σ_ε are the turbulent Prandtl numbers for k (turbulence kinetic energy) and ε (dissipation rate). The other notations are having their usual meaning.

The constants specified in FLUENT are $C_{2\varepsilon}$= 1.9, σ_k= 1 and σ_ε=1.2. The building was considered as a bluff body and flow around it was studied. The density of air is 1.224 kg/m^3. The inlet velocity was 10 m/s and the relative pressure at outlet was kept at 0 Pa. The turbulence intensity was considered to be 10%. While high resolution scheme was used for advection discretization, second order backward Euler scheme was used for transient discretization. For convergence, the root mean square (rms) target was set as 10^{-5}.

Vertical profiles of longitudinal velocity near Face A (see Fig. 2) for numerical and experimental studies is shown in Fig. 3(c). Power law of variation for velocity profile has been used. A similar variation along the height was kept for both numerical and experimental studies.

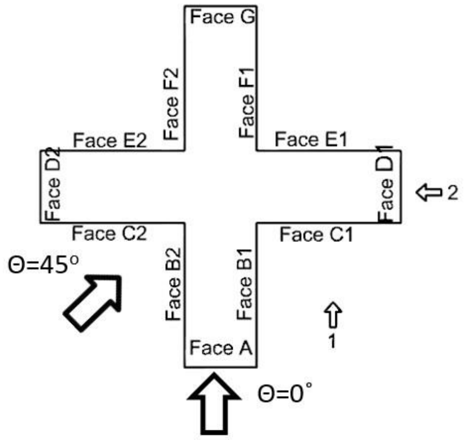

Fig. 2 Wind incident angle(θ) with respect to plan

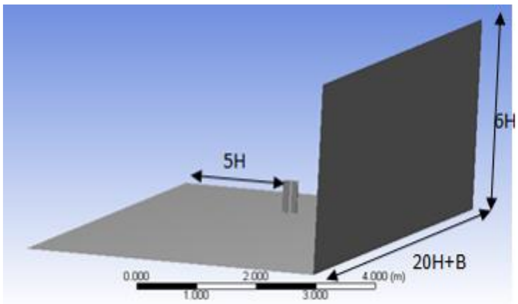

(a)

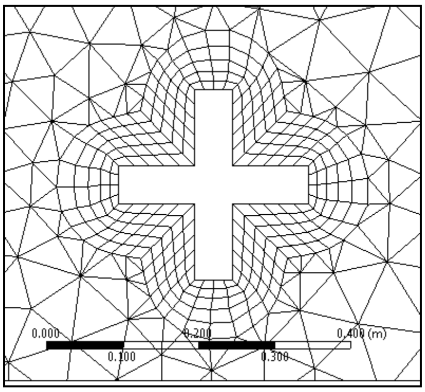

(b)

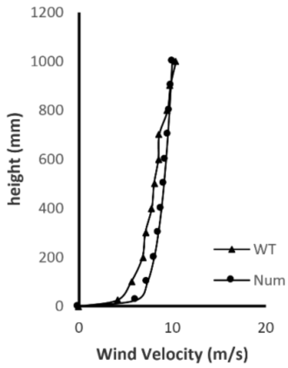

(c)

Fig. 3 (a) Details of computational domain, (b) Meshing pattern near the building surface and (c) Boundary layer velocity

4. Results and discussion

4.1 Wind incidence angle – 0˚

4.1.1 Numerically predicted wind flow

Fig. 4(a) shows the flow generated around the model (using k-ε model) for zero degree wind incidence angle. The flow pattern is symmetrical with two symmetrical vortices in the wake region. Velocity around the edges has increased due to separation of flow. The unsymmetrical pattern of flow after formation the vortices indicate the turbulent nature of flow. Thus any structure located in this zone will experience a dynamic loading due to vortex shedding (Fig. 4(a)). The flow, while using SST model, is almost identical with only significant difference observed in flow after formation of vortices (Fig. 4(b)). No asymmetry is present in this case and the peak velocity is little bit higher as compared to k-ε model.

The variation of flow along vertical direction of the building are shown in Figs. 5(a) and 5(b). While Fig. 5(a) shows the vertical wind profile around the structure generated from k-ε model, Fig. 5(b) shows the same for SST model. The flow predicted while using SST viscosity model seems more realistic.

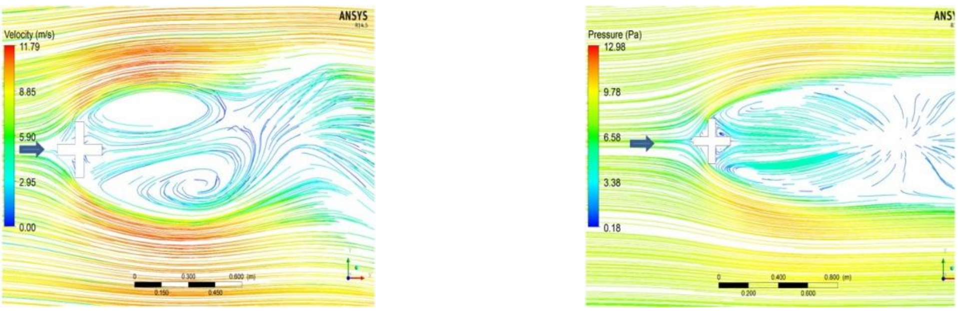

(a) (b)

Fig. 4 (a) Flow pattern around model for 0˚ wind incidence angle (k-ε model)- Plan and (b) Flow pattern around model for 0˚ wind incidence angle (SST model)- Plan

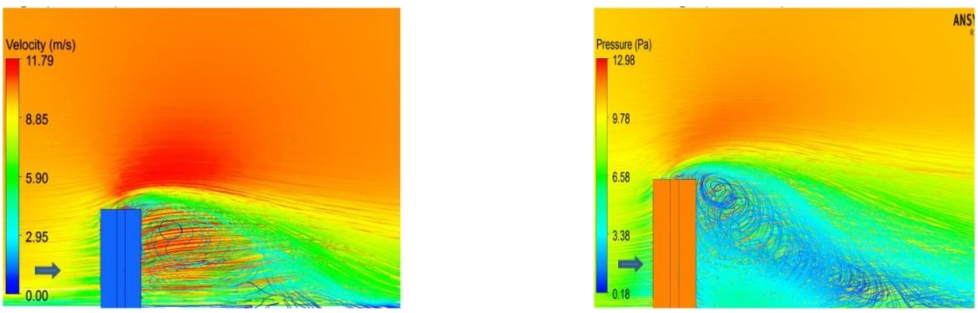

(a) (b)

Fig. 5 (a) Flow pattern around model for 0˚ wind incidence angle (k-ε model)- Elevation and (b) Flow pattern around model for 0˚ wind incidence angle (SST model)- Elevation

4.1.2 Pressure distribution

The model along with its different faces is already shown in Fig. 2. The contours for Faces A1, C1, E1 and G are observed from direction ‘1’ and that for Faces B1, D1 and F1 from direction ‘2’.

Figs. 6(a)-12(c) show the variation of mean pressure, represented in terms of pressure coefficient, on different faces of ‘+’ shaped building as obtained from k-ε and SST methods. Due to symmetry in flow pattern, the contour on symmetrical sides are identical. As observed from Figs. 6(a) and 6(b), Face A has experienced positive pressure with the maximum value (pressure coefficient of 0.986) around the middle width. The pressure near the surface edges is low due to separation of flow near the corners. The pressure distribution is symmetrical.

Unlike the case of a rectangular building where side face is subjected to negative pressure (i.e., suction), Face B1 (Figs. 7(a) and 7(b)) is mostly subjected to positive pressure with only a small portion around the top experiencing suction. This phenomenon is due to interference effect of Face C1. The flow of wind after striking Face C1 is reversed and results in positive pressure on Face B1. Moreover maximum pressure being concentrated near the Face C1 is also a result of the same flow reversal. As expected Face C1 (Figs. 8(a) and 8(b)) is subjected to positive pressure with high concentration zone located near Face D1. After the flow separation around the edge, Face D1 (Fig. 9(a) and 9(b)) experiences negative pressure with maximum pressure near Face C1. The leeward faces, namely E1, F1 and G, experiences suction with minimum pressure variation. On Faces F1 and F2 a bubble shape (Figs. 10(a) and10(b)) is formed near the edge due to irregular formation of eddies caused by separation of flow. The pressure also increases with height. Face G1 is having a symmetrical pressure distribution with maximum pressure near the top edge (Figs. 11(a) and 11(b)).

The contours obtained from the two analytical methods, viz. k-ε and SST are almost identical with SST yielding higher results.

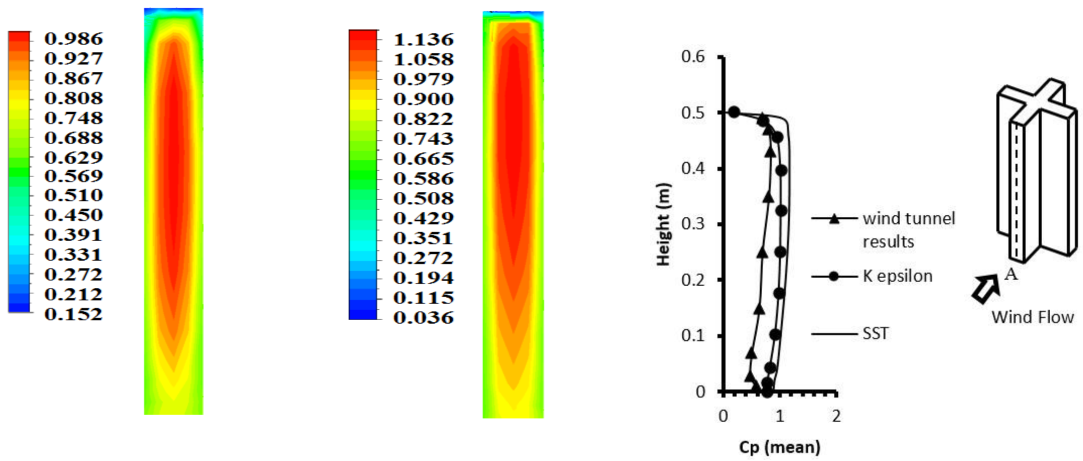

(a) (b) (c)

Fig. 6 (a) Pressure coefficient contour of Face A for 0˚ wind incidence angle (k-ε model), (b) Pressure coefficient contour of Face A for 0˚ wind incidence angle (SST model) and (c) Comparison of pressure coefficient along the vertical centreline for 0˚ incidence angle (Face A)

4.1.3 Numerical versus experimental results

The wind induced pressure coefficients along the horizontal and vertical lines are compared with the wind tunnel results. The general agreement among the result is quite good. Some discrepancies between the results along the horizontal centreline (Fig. 12(a)) for Faces B1 and B2 are noticed. This inconsistency between numerical and experimental result is probably due to the failure of numerical models to predict pressure variation occurring due to recirculation, caused by interference effect of Face C. Else, the results are quite close. The agreement is even better for horizontal line located near the top (Fig. 12(b)). The pressure coefficients along the vertical centreline (Figs. 6(c), 7(c), 8(c), 9(c), 10(c) and 11(c)) are also having reasonable agreement with the experimental results with the maximum difference on Face D1. The dispute in the results may be due to susceptibility of these edges to experimental conditions. The two analytical models, viz. k-ε and SST, yields almost same result in all the cases with only discrepancy noticed in case of Face D1 (Fig. 9(c)).

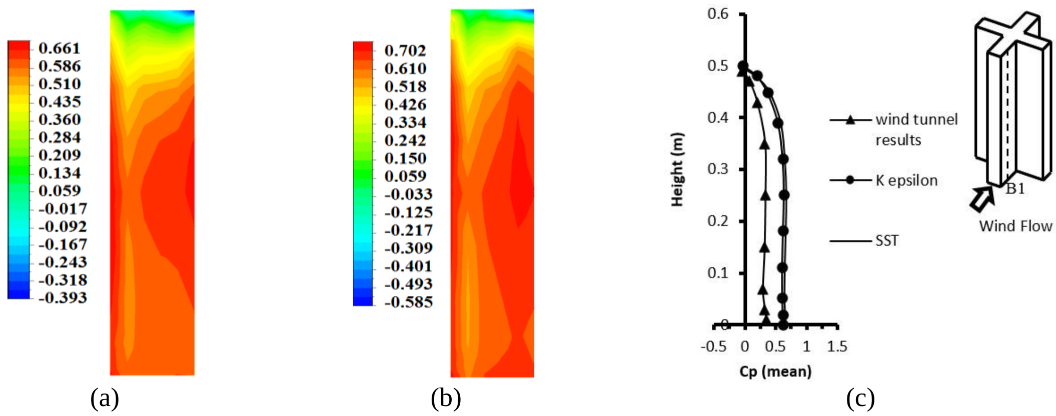

Fig. 7 (a) Pressure coefficient contour of Face B1 for 0˚ wind incidence angle (k-ε model), (b) Pressure coefficient contour of Face B1 for 0˚ wind incidence angle (SST model) and (c) Comparison of pressure coefficient along the vertical centreline for 0˚ incidence angle (Face B1)

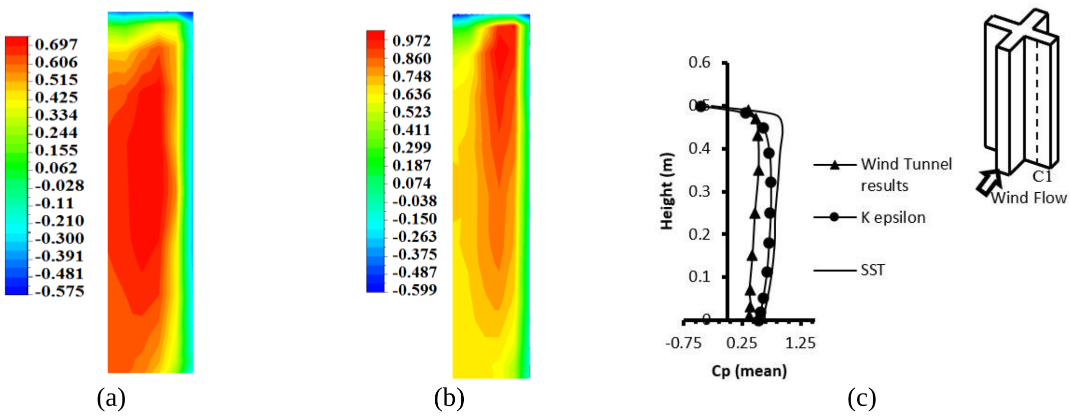

Fig. 8 (a) Pressure coefficient contour of Face C1 for 0˚ wind incidence angle (k-ε model), (b) Pressure coefficient contour of Face C1 for 0˚ wind incidence angle (SST model) and (c) Comparison of pressure coefficient along the vertical centreline for 0˚ incidence angle (Face C1)

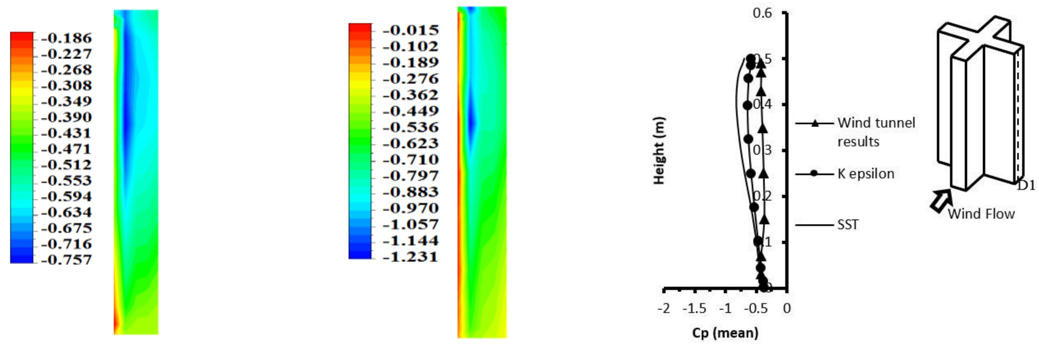

(a) (b) (c)

Fig. 9 (a) Pressure coefficient contour of Face D1 for 0˚ wind incidence angle (k-ε model), (b) Pressure coefficient contour of Face D1 for 0˚ wind incidence angle (SST model) and (c) Comparison of pressure coefficient along the vertical centreline for 0˚ incidence angle (Face D)

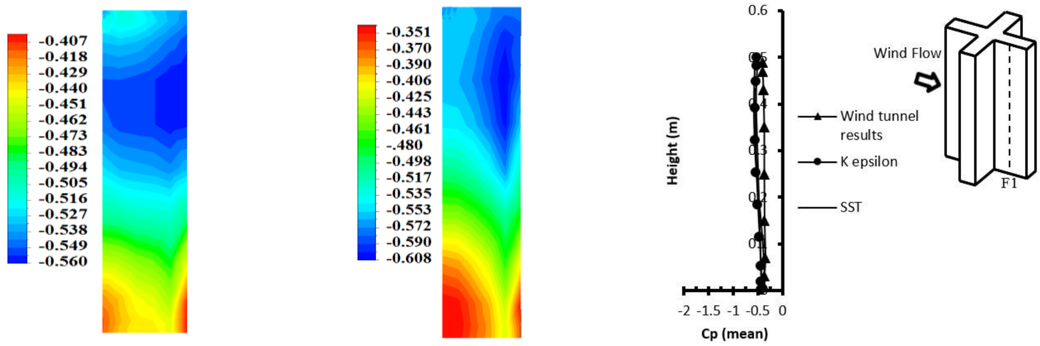

(a) (b) (c)

Fig. 10 (a) Pressure coefficient contour of Face F1 for 0˚ wind incidence angle (k-ε model), (b) Pressure coefficient contour of Face F1 for 0˚ wind incidence angle (SST model) and (c) Comparison of pressure coefficient along the vertical centreline for 0˚ incidence angle (Face F1)

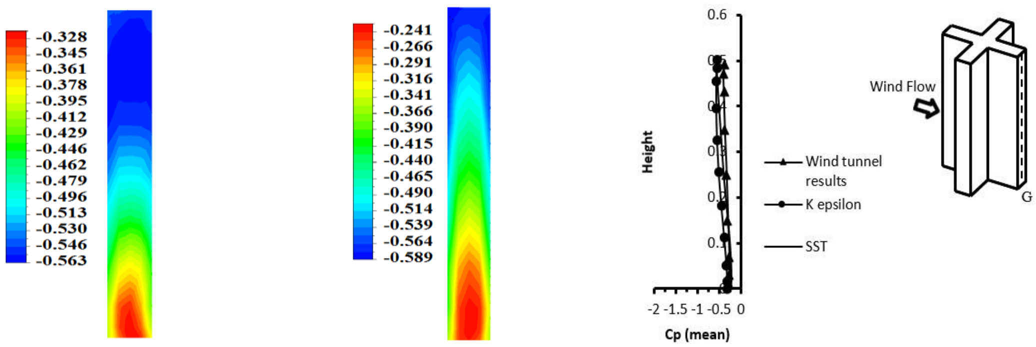

(a) (b) (c)

Fig. 11 (a) Pressure coefficient contour of Face G for 0˚ wind incidence angle (k-ε model), (b) Pressure coefficient contour of Face G for 0˚ wind incidence angle (SST model) and (c) Comparison of pressure coefficient along the vertical centreline for 0˚ incidence angle (Face G)

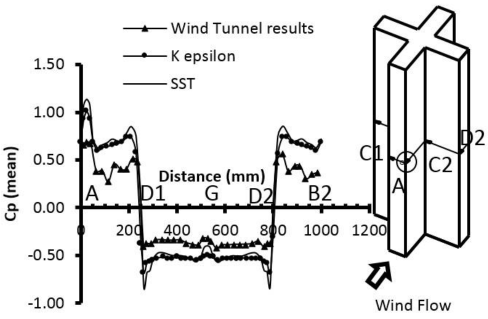

(a)

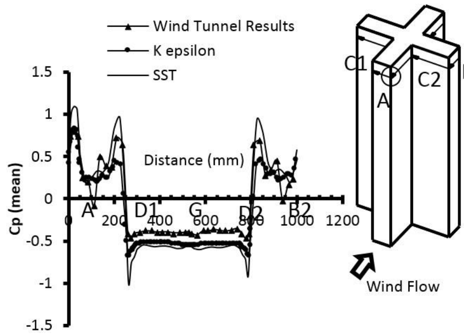

(b)

Fig. 12 (a) Comparison of pressure coefficient along the horizontal centreline for 0˚ incidence angle and (b) Comparison of pressure coefficient near top (30 mm below the top edge) for 0˚ incidence angle

4.2 Wind incidence angle – 45˚

4.2.1 Numerically predicted wind flow

The flow pattern around the model for 45˚ wind incidence angle is shown in Figs. 13(a) and 14(b). The wind flows sharply away from the corners of front surface and reverses after the corners. The flow is symmetrical with two symmetrical vortices forming in the wake region and two more vortices forming between the limbs of the '+' shaped model (Figs. 13(a) and 13(b)) due to interference effect by the inclined leeward side limbs. The flow pattern obtained using k-ε and SST models are similar.

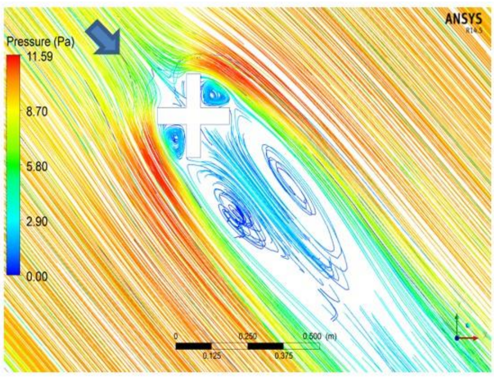

(a)

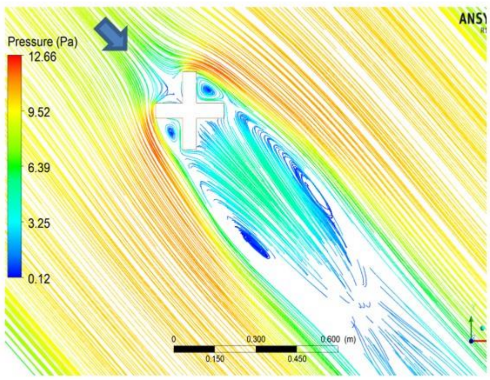

(b)

Fig. 13 (a) Flow pattern around model for 45˚ wind incidence angle (k-ε model)- Plan and (b) Flow pattern around model for 45˚ wind incidence angle (SST model)- Plan

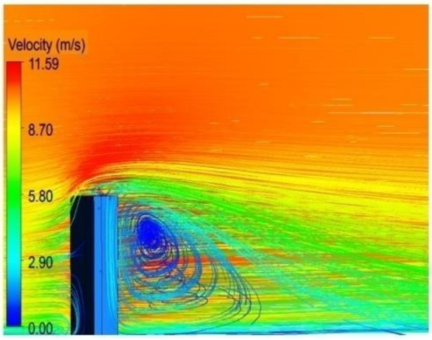

(a)

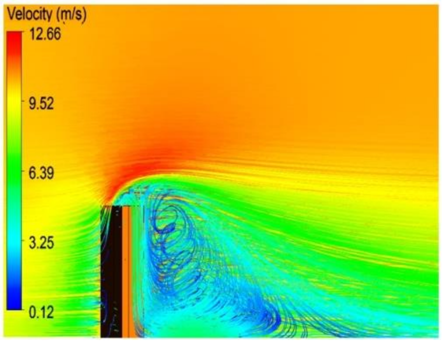

(b)

Fig. 13 (a) Flow pattern around model for 45˚ wind incidence angle (k-ε model)- Elevation and (b) Flow pattern around model for 45˚ wind incidence angle (SST model)- Elevation

Figs. 14(a) and 14(b) show the longitudinal sectional view of flow streamline around the model generated using k-ε and SST models respectively. The vortex formation on the rear side of the model is more prominent in the SST model as compared to k-ε model. The other features of flow are similar to that of the zero degree wind incidence angle.

4.2.2 Pressure distribution

The flow pattern for 45˚ wind incidence angle is also symmetrical and thus faces on symmetrical sides will have identical pressure distribution. The pressure distribution, represented in terms of pressure coefficients, on various faces are shown in Figs. 15(a)-18(c). The pattern of contours obtained using the two models are identical in most of the cases with only difference observed in case of Face B1.

Flow separation occurs near Face A and results in negative pressure. Only a small zone near the windward edge experiences positive pressure as observed from Fig. 15(a). Face B1 is subjected to negative pressure. A small bubble of high pressure zone is formed near the top (Figs. 16(a) and 16(b)) due to formation of vortex between Face B1 and C1 (Figs. 13(a) and 13(b)). A similar bubble has also formed on Face C1 (Figs. 18(a) and 18(b)). Face C2 experiences positive pressure with maximum pressure concentrated towards B2 as evident from Figs. 17(a) and 17(b). As expected, Faces D1 and E1 (i.e., inclined leeward side faces) are subjected to suction and almost no pressure variation along the horizontal line is observed.

4.2.3 Numerical versus experimental results

The mean pressure coefficients obtained from numerical study along the horizontal and vertical line are compared with wind tunnel results (Figs. 15(c), 16(c), 17(c), 18(c), 19(a) and 19(b)). The test results are in good agreement with numerical results. For Face A, the pressure coefficients along vertical centreline obtained from k-ε model are almost equal to the pressure coefficients from wind tunnel test (Fig. 15(c)) with SST model yielding comparatively higher value. The results along horizontal centreline are also in close proximity (Fig. 19(a)). However there are some discrepancies (about 25%) in pressure coefficients obtained by experimental and numerical methods near the top surface for B1 and E2 (Fig. 19(b)). This is probably due to susceptibility of the pressure tapping points to detect pressure variation due to separation of flow from top edge.

5. Conclusions

Present study has showed that irregular plan shaped buildings are subjected to different pressure distribution, as compared to regular plan shaped buildings after distribution. Moreover with change in wind angle the negative pressure (suction) induced may change drastically. The interference effect on different parts is also to be kept in mind while calculating the wind load on buildings or any other important structures. The significant outcomes of this present study on '+' plan shaped tall buildings can be summarized as follow:

1. The pressure distribution on a Face B1 and B2 for zero degree wind incidence angle is drastically changed due to interference effect of Face C1 and C2 respectively.
2. A thin line of high suction pressure (maximum pressure coefficient of -0.75) is observed on Face D1 and D2 for zero degree wind incidence angle.
3. The rear faces (viz. E1, E2, F1, F2 and G) are subjected to uniform negative pressure (suction) along both horizontal and vertical line for 0˚ angle of attack.
4. The nature of wind pressure on Face A, B1 and C1 have reversed for 45˚ angle of attack. The above faces are subjected to positive pressures for 0˚ wind incidence angle whereas negative pressures are observed for 45˚ incidence angle.
5. Apart from the two vortices in wake region, two more vortices are formed between Faces B1, C1 and E2, F2 for 45˚ incidence angle.
6. A small bubble of high negative pressure (maximum pressure coefficient of -0.9) is developed towards the top of Face B1 and C1 due to formation vortex for 45˚ wind angle.
7. Faces D1, E1, F1 and G are subjected to uniform negative pressure along horizontal line for 45˚ angle of attack.
8. The negative pressure on Face D1 is reduced by 36% for 45˚ wind incidence angle as compared to 0˚ wind angle.
9. The pressure on Faces B2 and C2 is increased by about 64% for wind incidence angle of 45˚ as compared to 0˚ wind angle.
10. The pressure on the leeward sides for both wind incidence angles are almost same.

The results obtained from numerical methods have shown a general good agreement with experimental study. Although there are some discrepancies, the numerical results along with the experimental results can provide fair amount of idea regarding wind load on such irregular structures.

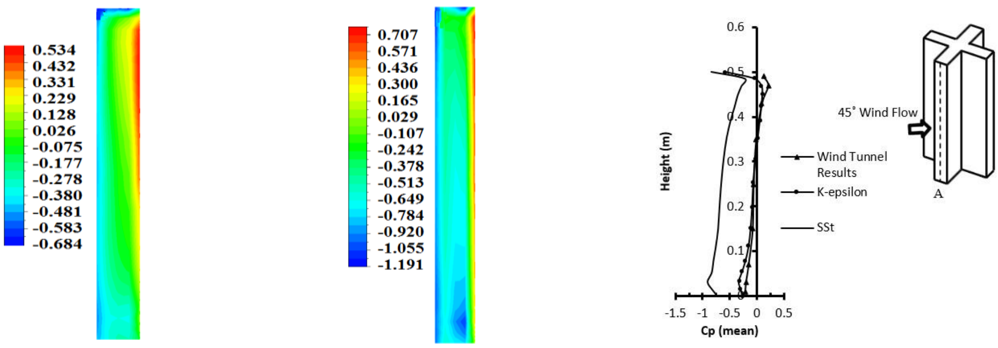

(a) (b) (c)

Fig. 15 (a) Pressure coefficient contour of Face A for 45˚ wind incidence angle (k-ε model), (b) Pressure coefficient contour of Face A for 45˚ wind incidence angle (SST model) and (c) Comparison of pressure coefficient along the vertical centreline for 45˚ incidence angle (Face A)

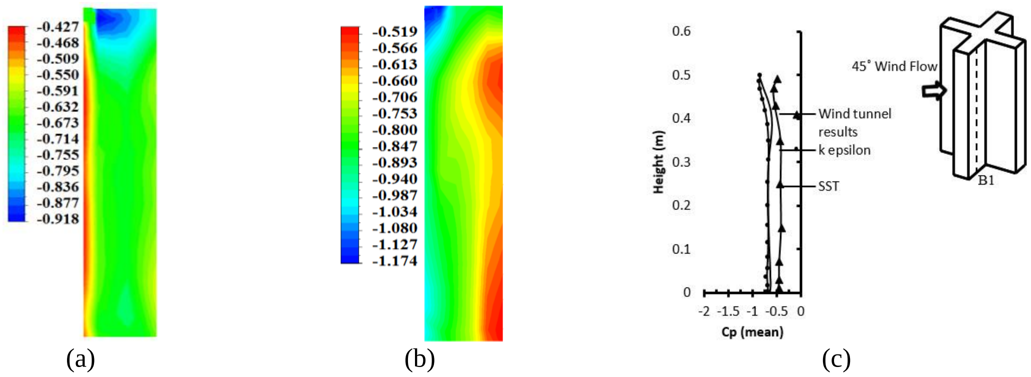

Fig. 16 (a) Pressure coefficient contour of Face B1 for 45° degree wind incidence angle (k-ε model), (b) Pressure coefficient contour of Face B1 for 45° degree wind incidence angle (SST model) and (c) Comparison of pressure coefficient along the vertical centreline for 45° incidence angle (Face B1)

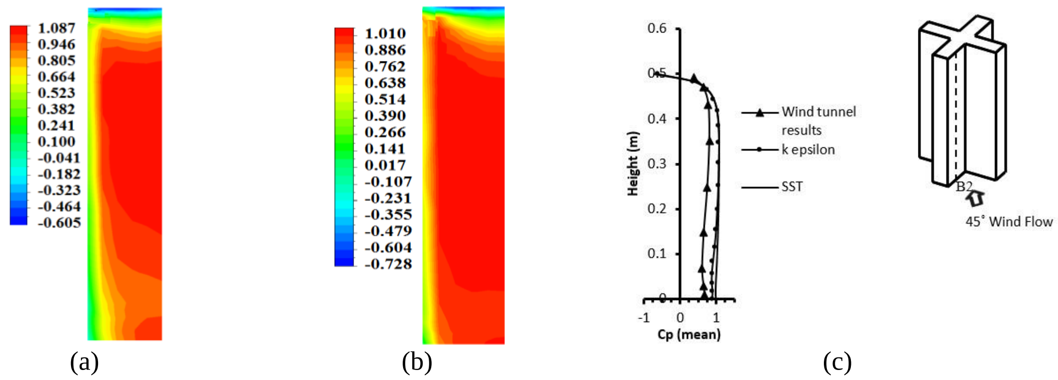

Fig. 17 (a) Pressure coefficient contour of Face C2 for 45° degree wind incidence angle (k-ε model), (b) Pressure coefficient contour of Face C2 for 45° degree wind incidence angle (SST model) and (c) Comparison of pressure coefficient along the vertical centreline for 45° incidence angle (Face C2)

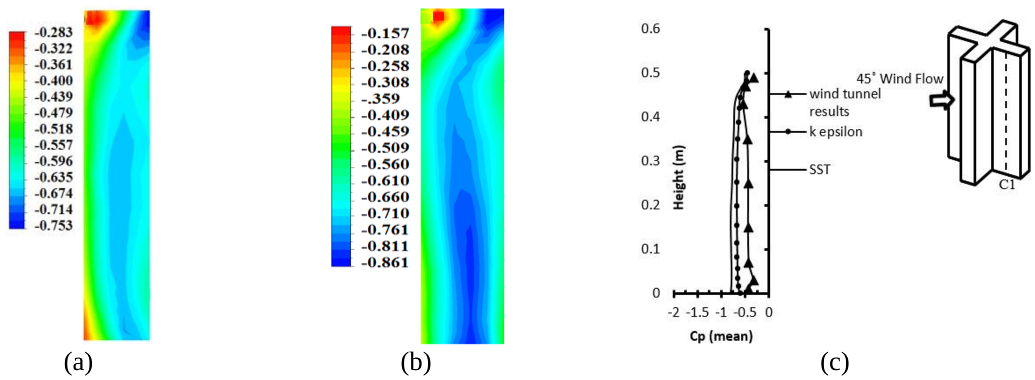

Fig. 18 (a) Pressure coefficient contour of Face C1 for 45° degree wind incidence angle (k-ε model), (b) Pressure coefficient contour of Face C1 for 45° wind incidence angle (SST model) and (c) Comparison of pressure coefficient along the vertical centreline for 45° incidence angle (Face C1)

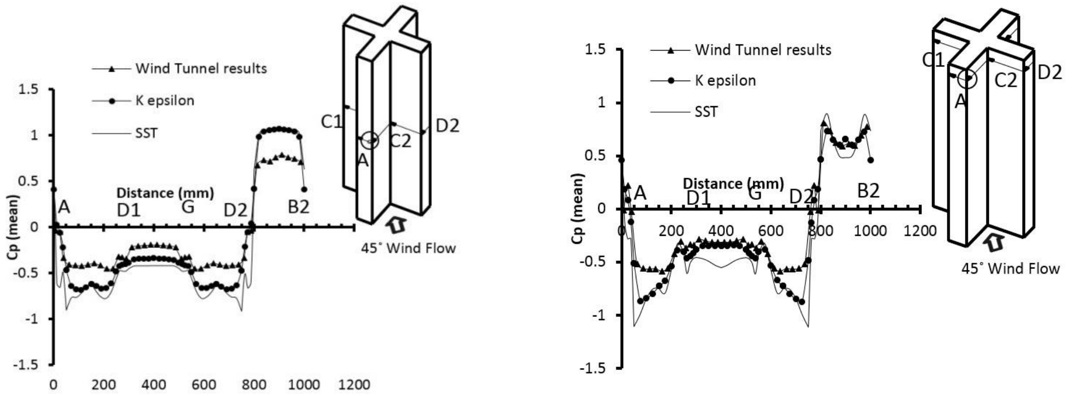

(a) (b)

Fig. 19 (a) Comparison of pressure coefficient along the horizontal centreline for 45˚ incidence angle and (b) Comparison of pressure coefficient near top for 45˚ incidence angle

Acknowledgements

The authors would like to express their sincere gratitude to Department of Science & Technology, Govt. of India for funding the research work and to Indian Institute of Technology, Roorkee for providing the experimental setup.

References

Amin, J.A. and Ahuja, A.K. (2012), “Wind-induced mean interference effects between two closed spaced buildings”, *Korean Soc. Civil. Eng*., **16**(1), 119-131.

AS/NZS: 1170.2 (2002), *Structural design actions, part 2: wind actions*, Standards Australia/Standards New Zealand, Sydney, Wellington.

ASCE: 7-02 (2002), *Minimum design loads for buildings and other structures*, Structural Engineering Institute of the American Society of Civil Engineering, Reston.

Balendra, T., Anwar, M.P. and Tey, K.L. (2005), “Direct measurement of wind-induced displacements in tall building models using laser positioning technique”, *J. Wind Eng. Ind. Aerod*., **93**(5), 399-412.

Blocken, B. and Carmeliet, J. (2005), “High resolution wind-driven rain measurements on a low-rise building-experimental data for model development and model validation”, *J. Wind Eng. Ind. Aerod*., **93** (12), 905-928.

Braun, A.L. and Awruch, A.M. (2009), “Aerodynamic and aeroelastic analyses on the CAARC standard tall building model using numerical simulation”, *J. Wind Eng. Ind. Aerod.*, **87**(9-10), 564-581.

Cheng, C.K.C., Lam, K.M., Leung, Y.T.A., Yang, K., Li Danny, H.W. and Cheung Sherman, C.P. (2011), “Wind-induced natural ventilation of re-entrant bays in a high-rise building”, *J. Wind Eng. Ind. Aerod.*, **99** (2-3), 79-90.

Dagnew, A.K., Bitsuamalk, G.T. and Merrick, R. (2009), “Computational evaluation of wind pressures on tall buildings”, *Proceedings of the 11th Americas Conference on Wind Engineering*, San Juan, Puerto Rico, June 22-26.

Davenport, A.G. (1993), *The response of slender structures to wind*, Wind Climate in Cities, (Ed. Cermak *et al*.), Germany.

Franke, J., Hirsch, C., Jensen, A., Krüs, H., Schatzmann, M., Westbury, P., Miles, S., Wisse, J. and Wright, N.G. (2004), *Recommendations on the use of CFD in wind engineering*, COST Action C14: Impact of Wind and Storm on City Life and Built Environment, von Karman Institute for Fluid Dynamics.

Fu, J.Y., Li, Q.S., Wu, J.R., Xiao, Y.Q. and Song, L.L.(2008), "Field measurement of boundary layer wind characteristics and wind induced response of super tall buildings", *J. Wind Eng. Ind. Aerod*., **96**(8-9), 1332-1358.

Gomes, M., Rodrigues, A. and Mendes, P. (2005), "Experimental and numerical study of wind pressure on irregular-plan shapes", *J. Wind Eng. Ind. Aerod.*, **93**(10), 741-756.

Gu, M. (2009), "Study on wind loads and responses on tall buildings and structures", *Proceedings of the Seventh Asia Pacific Conference*, November- 8-12, 2009, Taipei, Taiwan.

IS: 875 (1987), *Indian standard code of practice for design loads (other than earthquake) for buildings and structures, part 3 (wind loads),* Bureau Of Indian Standards, New Delhi.

Kim, Y., You, K. and Ko, N. (2008), "Across-wind responses of an aeroelastic tapered tall building", *J. Wind Eng. Ind. Aerod*., **96**(8-9), 1307-1319.

Kwok, K.C.S. (1988), "Effect of building shape on wind-induced response of tall building", *J. Wind Eng. Ind. Aerod.*, **28**(1-3), 381-390.

Kwok, K.C.S., Qin, X.R., Fok, C.H. and Hitchcock, P.A. (2011), "Wind-induced pressures around a sectional twin-deck bridge model: effects of gap-width on the aerodynamic forces and vortex shedding mechanisms", *J. Wind Eng. Ind. Aerod.*, **110**, 50-61.

Lin, N., Letchford, C., Tamura, Y. and Liang, B. (2004), "Characteristics of wind forces acting on tall buildings", *J. Wind Eng. Ind. Aerod.*, **93**, 217-242.

Mendis, P., Ngo, T., Haristos, N., Hira, A., Samali, B. and Cheung, J. (2007), "Wind loading on tall buildings", *Electron. J. Struct. Eng*., Special issues, 41-54.

NBC (Part-4) (1995), *Structural commentaries*, National Research Council of Canada.

Revuz, J., Hargreaves, D.M. and Owen, J.S. (2012), "On the domain size for steady state CFD modelling of tall building", *Wind Struct*., **15**(4), 313-329.

Simiu, E. and Scanlan, R.H. (1996), *Wind effects on structures*, 2nd Ed, John Wiley & Sons, New York.

Spence, M.J.S. and Gioffrè, M. (2012), "Large scale reliability-based design optimization of wind excited tall buildings", *Probabilist. Eng. Mech*., **28**, 206-215.

Stathopoulos, T. and Baniotopoulos, C.C. (2007), *Wind effects on buildings and design of wind-sensitive structures*, Springer Wien New York, Udine, Italy.

Song, M.X., Chen, K., He, Z.Y. and Zhang, X. (2014) "Wind resource assessment on complex terrain based on observations of a single anemometer", *J. Wind Eng. Ind. Aerod*., **125**, 22-29.

Zhou, Y., Kijewski, T. and Kareem, A. (2002), "Along-wind load effects on tall buildings: comparative study of major international codes and standards", *J. Struct. Eng. - ASCE*, **128**, 788-796.

CC